

A.J. BERGLUND 
H. MABUCHI

Performance bounds on single-particle tracking by fluorescence modulation

Physical Measurement and Control 266-33, California Institute of Technology, Pasadena, CA 91125, USA

Received: 2 November 2005

Published online: 14 January 2006 • © Springer-Verlag 2005

ABSTRACT We consider fundamental bounds on the performance of single-particle tracking schemes based on non-imaging, fluorescence modulation methods. We calculate the noise density of a linearized position estimate arising from photon-counting statistics and find the optimal estimate of a freely diffusing particle's position in the presence of this noise. For the experimentally relevant case of a Gaussian laser rapidly translated in a circular pattern, explicit expressions are derived for the noise density. Tracking performance limits are obtained by considering the variance in the estimated position of a Brownian particle with diffusion coefficient D in the presence of a noise density n_m , which we find scales generically as $\sqrt{Dn_m^2}$. For reasonable experimental parameters, a particle with diffusion coefficient $D = 1 \mu\text{m}^2/\text{s}$ cannot be tracked with accuracy better than approximately 100 nm in three dimensions or 80 nm in two dimensions. Using a combination of exact results and numerical simulation, we construct a 'phase diagram' for determining parameter regimes in which a particle can be tracked in the presence of measurement noise.

PACS 87.64.Tt; 87.64.Ni; 87.15.Vv

1 Introduction

Recent theoretical [1–6] and experimental [7–10] results have established the feasibility of tracking a single fluorescent particle in a confocal or epifluorescence microscope using non-imaging fluorescence modulation techniques. These techniques use a spatial modulation of the excitation intensity to encode a particle's position in some frequency component of the fluorescence signal. A suitable feedback control law is then applied in order to lock the particle's position to the centroid of the excitation intensity. Since the fluorescence signal is fundamentally noisy, any estimate of the particle's position based on this signal also inherits this noise. For a static particle, this uncorrelated noise can be removed by sufficient temporal averaging (both for imaging and non-imaging techniques), a fact exploited to achieve nanometer fluorescent particle localization [11]. However, if a particle moves during the measurement, either stochastically or in an

unknown deterministic way, the fluorescence noise results in a fundamental limit on the accuracy with which its position can be determined. Roughly speaking, a fast particle cannot be localized as accurately as a slow particle. In tracking applications, if a particle cannot be sufficiently localized within the characteristic tracking time scale, then it cannot be tracked at all. In this paper, we consider these fundamental constraints, and we place upper limits on the performance of particle tracking by fluorescence modulation in the presence of photon-counting noise. Whereas the finite bandwidth response of a realistic actuator was considered in previous work [5, 6], here we consider tracking performance limits based solely on photon-counting statistics. The paper is organized as follows. In Sect. 2 we derive a simple expression for the noise spectral density in a fluorescence modulation measurement and, in Sect. 3, we consider the statistical task of estimating a moving particle's position by filtering a noisy measurement. In Sect. 4, we present the results of numerical simulations of the tracking process and give a qualitative method for determining the parameter regimes in which a particle can be tracked.

2 Noise spectral density of linear position estimation

In this section, we are concerned with finding the noise spectral density associated with position estimation by fluorescence modulation and demodulation techniques. For concreteness, we will derive results for our own experimental geometry [5, 10]. Our arguments generalize in a straightforward way to different experimental geometries. Consider a particle's two-dimensional position in the xy plane (or equivalently the $\varrho\theta$ plane in polar coordinates), in which a Gaussian excitation laser is translated in a circular pattern. The rate of fluorescence from a particle at position $\mathbf{x} = (x, y) \leftrightarrow (\varrho, \theta)$ is given by

$$\Gamma_x(t) = \Gamma_0 \exp \left\{ -2 \left[\frac{\varrho^2}{w^2} + \frac{r_0^2}{w^2} - 2 \frac{r_0\varrho}{w^2} \cos(\theta - \omega_0 t) \right] \right\}, \quad (1)$$

where Γ_0 is the peak fluorescence rate, w is the beam waist, r_0 is the radius of rotation of the beam, and ω_0 is the angular rotation frequency.

In our experiment [10], the actual fluorescence signal is a stochastic train of voltage pulses from the output of a single-

✉ Fax: +1-626-395-3802, E-mail: berglund@caltech.edu

photon counter, with the arrival times of the pulses governed by the rate $\Gamma_x(t)$. Let $V(t)$ denote the shape of the electronic pulses, t_k denote the k th photon pulse arrival time, and let

$$T(t) = \sum_{k=1}^{\infty} \delta(t - t_k). \quad (2)$$

Here $T(t)$ is the time derivative of a stochastic point process whose statistics are governed by the time-dependent rate $\Gamma_x(t)$. The relationship between these functions is given by standard properties of the Poisson process [12, 13]:

$$E[T(t)] = \Gamma_x(t), \quad (3a)$$

$$E[T(t_1)T(t_2)] = \Gamma_x(t_1)\Gamma_x(t_2) + \Gamma_x(t_1)\delta(t_1 - t_2), \quad (3b)$$

where $E[\cdot]$ denotes the expectation value over realizations of $T(t)$. The full stochastic fluorescence signal $s(t)$ is given by a convolution integral

$$s(t) = (T * V)(t) \equiv \int_{-\infty}^{\infty} V(t - t')T(t') dt'. \quad (4)$$

In order to estimate the particle's position x , we must extract the component of $s(t)$ [actually the component of $\Gamma_x(t)$] at the laser rotation frequency ω_0 . We assume that ω_0 is much faster than the time scale of the particle's motion, so that over a single rotation period the particle can be considered to be stationary. Furthermore, we assume that the voltage pulses are very narrow (in time) compared to all other frequencies of interest, so that we may write $V(t) \approx V_0\delta(t)$ or equivalently $s(t) \approx V_0T(t)$ ¹. We define the 'instantaneous' component of $s(t)$ at angular frequency ω to be

$$\begin{aligned} \tilde{s}_t(\omega) &= \int_t^{t+2\pi/\omega_0} e^{-i\omega u} s(u) du \\ &\approx V_0 \int_t^{t+2\pi/\omega_0} e^{-i\omega u} T(u) du \equiv V_0 \tilde{T}_t(\omega), \end{aligned} \quad (5)$$

where $\tilde{T}_t(\omega)$ is the finite-windowed Fourier transform of $T(t)$, over one rotation period $2\pi/\omega_0$ beginning at time t . The real and imaginary parts of $\tilde{s}_t(\omega)$, or at least a bandwidth-limited filtration of these components, can be measured using phase-sensitive lock-in detection. These measurements probe a time-dependent, stochastic frequency spectrum $\tilde{s}_t(\omega)$. Again using Eqs. (3a) and (3b), we calculate the expectation value of the component of $s(t)$ at $n\omega_0$, where n is a positive integer:

$$E[\tilde{s}_t(n\omega_0)] = V_0 E[\tilde{T}_t(n\omega_0)] = V_0 h_n(\varrho) e^{in\theta}, \quad (6)$$

with

$$h_n(\varrho) = 2\pi \frac{\Gamma_0}{\omega_0} \exp\left[-\frac{2}{w^2}(r_0^2 + \varrho^2)\right] I_n\left(\frac{4r_0\varrho}{w^2}\right). \quad (7)$$

Here I_n is the n th-order modified Bessel function. For $\varrho/w \ll 1$ and $\varrho r_0/w^2 \ll 1$ (we will further assume that $r_0 \sim w$), we may write

$$h_n(\varrho) \approx \frac{2\pi}{n!} \left(\frac{\Gamma_0}{\omega_0}\right) \left(\frac{2\varrho r_0}{w^2}\right)^n \exp\left[-2\frac{r_0^2}{w^2}\right] + O\left(\frac{\varrho}{w}\right)^{n+1}. \quad (8)$$

Equation (8) for $h_1(\varrho)$ shows that the component of $s(t)$ at frequency ω_0 is, on average, linear in the radial coordinate ϱ near the origin. Information about the angular coordinate θ is contained in the complex exponential phase, whose real and imaginary parts are accessible by lock-in detection. Near the origin, the real part of $\tilde{s}_t(\omega_0)$ is linear in the particle's x coordinate and the imaginary part is linear in the y component (on average). This linear dependence of the mean values of $\tilde{s}_t(\omega_0)$ near the origin provides the error signal for lock-in detection. Furthermore, the time-averaged excitation intensity is given by the $n = 0$ component, $\tilde{s}_t(0)$, while the variance will be shown to depend on the $n = 2$ component. The error signal $h_1(\varrho)$ together with its linear approximation and the average intensity $h_0(\varrho)$ are shown in Fig. 1 for two values of the offset parameter r_0/w .

Let us now construct an explicit estimator of the (stationary) particle's x position based on the measured frequency component $\tilde{s}_t(\omega_0)$. An analogous argument will hold for the y component. Note that measurement noise results in a time-dependent position estimate even for a stationary particle, so we must continue to use the subscript t . Let us define a reciprocal distance k_x by

$$k_x = 4\pi \left(\frac{\Gamma_0}{\omega_0}\right) \left(\frac{r_0}{w^2}\right) \exp\left[-2\frac{r_0^2}{w^2}\right], \quad (9)$$

so that

$$E\{\text{Re}[\tilde{s}_t(\omega_0)]\} = \text{Re}\{E[\tilde{s}_t(\omega_0)]\} \approx V_0 k_x x. \quad (10)$$

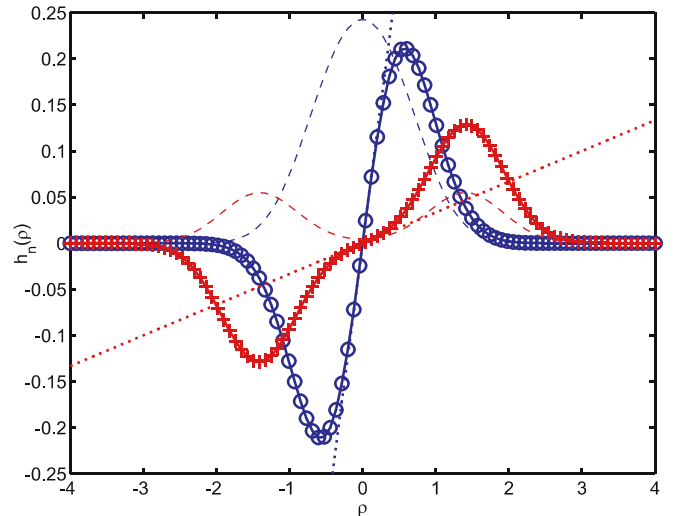


FIGURE 1 The error signal function $h_1(\varrho)$ for $r_0 = 0.5$ (blue \circ) and $r_0 = 1.5$ (red $+$), with $w = 1$ and $2\pi\Gamma_0/\omega_0 = 1$. The dotted lines are the linear approximation of Eq. (8), while the dashed lines show the time-averaged laser intensity given by $h_0(\varrho)$ (arbitrary units)

¹ For our experiments, we use avalanche photodiodes with a pulse width of approximately 25 ns, while the rotation period is 125 μ s, so that this approximation is quite valid.

Now we can construct our stochastic, time-dependent estimate \hat{x}_t of the particle's position x :

$$\hat{x}_t = \frac{2\pi B}{V_0 k_x \omega_0} \operatorname{Re} \int_t^{t+1/B} e^{-i\omega_0 u} s(u) du. \quad (11)$$

In Eq. (11), B is the filter bandwidth, which is assumed to be much larger than the rotation frequency $\omega_0/2\pi$; with this separation of time scales, we may make the approximation $\omega_0/2\pi B \approx N$, where N is a (large) integer. \hat{x}_t has the desired property that

$$E[\hat{x}_t] \approx \varrho \cos \theta = x \quad (12)$$

near the origin (since the average signal is periodic at the rotation frequency ω_0 , an integral over N periods is just N times the integral over a single period), which is why it is useful as an error signal for locking the particle's position to the origin using feedback control.

We are now in a position to derive the primary result of this section. We may find the estimator variance, or squared tracking error, \hat{x}_t , by substituting into the preceding formulas to find that

$$E[(x - \hat{x}_t)^2] = \frac{1}{2Nk_x^2} [h_0(\varrho) + h_2(\varrho) \cos \theta] \approx \frac{h_0(\varrho)}{2Nk_x^2}, \quad (13)$$

where the approximation is valid in the linear regime near the origin. The right-most expression in Eq. (13) does not depend on ϱ , since $h_0(\varrho)$ also does not, so, substituting back in for N and $h_0(\varrho)$, we find that

$$E[(x - \hat{x}_t)^2] = \left[w \psi \left(\frac{r_0}{w} \right) \sqrt{\frac{B}{\Gamma_0}} \right]^2, \quad \psi(x) = \frac{1}{\sqrt{8}} \frac{e^{-x^2}}{x}, \quad (14)$$

where ψ is a dimensionless function characterizing the beam geometry. The standard deviation in the tracking error scales as \sqrt{B} , a characteristic feature of shot-noise processes. The measurement noise density n_m arising from photon-counting statistics is given by

$$n_m = \frac{\sqrt{E[(x - \hat{x}_t)^2]}}{\sqrt{B}} = \psi \left(\frac{r_0}{w} \right) \frac{w}{\sqrt{\Gamma_0}}, \quad (15)$$

which has dimensions of (for example) $\mu\text{m}/\sqrt{\text{Hz}}$. This noise spectral density is valid for feedback bandwidths B that are large compared to the rotation frequency ω_0 . However, note that ω_0 appears nowhere within the expression for n_m , so that we are free to make ω_0 arbitrarily large with no effect on the noise figure. Also, note that a similar noise figure will apply to noise in the measurement of each Cartesian component of the particle's position (for the case described here, the noise figures for x and y detection are identical).

The specific form of $\psi(x)$ was derived for our particular experimental geometry. For this case, $\psi(r_0/w)$ achieves its minimum value at $r_0/w = 1/\sqrt{2}$, where $\psi(1/\sqrt{2}) = \psi_{\text{opt}} \approx 0.82$. Recall that the expression for the noise density is only

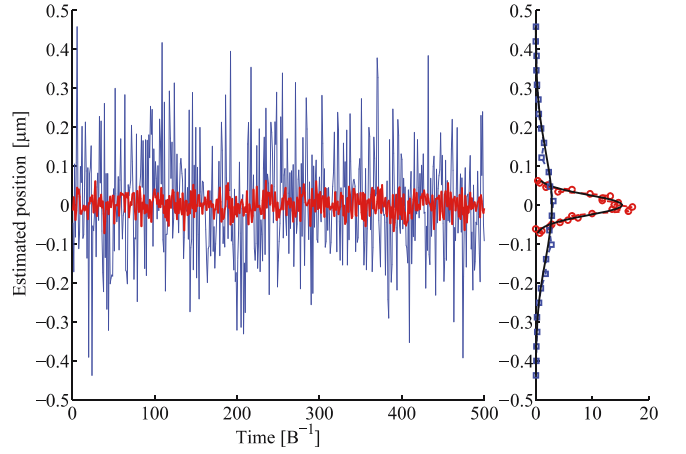


FIGURE 2 (Left) Numerical simulation of the estimate \hat{x}_t of a particle's position based on fluorescence demodulation. The particle was fixed at the coordinate origin. The red, more localized results are for $r_0/w = 1/\sqrt{2}$, $w = 1 \mu\text{m}$, $\Gamma_0 = 10^5 \text{ s}^{-1}$, and $\Gamma_B = 0$. The blue, wider distribution was computed with $r_0/w = 1.4$, $\Gamma_0 = 10^5 \text{ s}^{-1}$, and $\Gamma_B = 10^4 \text{ s}^{-1}$. For both curves, the laser rotation period was $\omega_0 = 2\pi \times 8 \text{ kHz}$ and the bandwidth was $B = 100 \text{ Hz}$. (Right) Simulated distributions together with those predicted by $n_m \sqrt{B}$ as calculated in the text

valid in the linear regime $\varrho/w \ll 1$ together with the additional assumption that $r_0 \sim w$, but ψ_{opt} is accessible well within this regime.

If we add a finite background count rate Γ_b to $\Gamma_x(t)$ and carry out the same analysis, we find a measurement noise density $n_m \rightarrow \sqrt{n_m^2 + n_b^2}$, where the background contribution to the measurement noise density is

$$n_b = \psi \left(\frac{\sqrt{2}r_0}{w} \right) w \sqrt{\frac{2\Gamma_b}{\Gamma_0^2}}. \quad (16)$$

Finally, note that the results derived here require only the linear relationship between the frequency components of $s(t)$ and the particle's position near the origin, which is an essential ingredient for linearizing and locking a nonlinear system using feedback control. For a different experimental geometry, or tracking in higher dimensions, these methods can be applied in exactly the same way to derive the measurement noise spectral density n_m for each Cartesian coordinate. A simulation of the position estimator \hat{x}_t applied to a stationary particle at the coordinate origin is shown in Fig. 2.

3 Optimal position estimation

In Sect. 2, we derived a noise spectral density n_m by considering the effect of photon-counting statistics on fluorescence demodulation measurements. This noise density determines the standard deviation in estimating a stationary particle's position in a time $1/B$ to be $n_m \sqrt{B}$: a static particle can be localized arbitrarily well by averaging the measurement for a sufficiently long time. In this section, we will take the noise spectral density n_m as given and consider position estimation of a diffusing particle. For this case, there exist an optimal bandwidth and a finite lower bound on the noise in the particle's estimated position. In the first part of this section, we will calculate the localization noise for a first-order low-pass filtration of a diffusing particle's position plus

measurement noise. We will find the optimal bandwidth and minimum localization noise for this case. We will discuss particle position estimation and particle tracking control interchangeably, since we are interested here in fundamental tracking limits where we assume that the tracking control apparatus can respond instantaneously to the optimal estimate². Therefore, optimal estimation results are equivalent to optimal control results for this idealized case.

Consider the time-dependent position X_t of a particle diffusing in one dimension with diffusion coefficient D . If we measure this particle's position with noise n_m and then form our estimate \hat{X}_t of the particle's position by filtering the result at a bandwidth B , we find the following coupled stochastic differential equations for X_t and \hat{X}_t :

$$d \begin{pmatrix} X_t \\ \hat{X}_t \end{pmatrix} = \begin{pmatrix} 0 & 0 \\ -B & B \end{pmatrix} \begin{pmatrix} X_t \\ \hat{X}_t \end{pmatrix} dt + \begin{pmatrix} \sqrt{2D} & 0 \\ 0 & n_m B \end{pmatrix} \begin{pmatrix} dW_1 \\ dW_2 \end{pmatrix}, \quad (17)$$

where dW_1 and dW_2 are independent stochastic Wiener increments [13] driving the particle's diffusion and the measurement noise, respectively. Equations (17) represent a two-dimensional Ornstein–Uhlenbeck process where the components have an obvious interpretation in terms of the particle's position and the estimated position. Since the Ornstein–Uhlenbeck process is Gaussian, the particle's position will remain Gaussian distributed so long as its initial position is either deterministic or Gaussian distributed as well. We may collapse Eqs. (17) to a single equation for the measurement error $e_t = X_t - \hat{X}_t$:

$$de_t = -Be_t dt + \sqrt{2\bar{D}} dW, \quad \bar{D} = D + \frac{n_m^2 B^2}{2}, \quad (18)$$

which is a simple one-dimensional Ornstein–Uhlenbeck process with effective diffusion coefficient \bar{D} . Equation (18) suggests that a particle tracked at bandwidth B looks (statistically) like a freely diffusing particle tracked with no measurement noise, but with an effectively larger diffusion coefficient \bar{D} given by the sum of D and the contribution from measurement noise $n_m^2 B^2/2$.

We are interested in steady-state tracking, not transient behavior during the locking process, so we will use steady-state solutions. For long times compared to the feedback time scale $1/B$, we find that $E[e_t] = 0$ and

$$E[e_t^2] = \frac{\bar{D}}{B} = \frac{D}{B} + \frac{n_m^2 B}{2}. \quad (19)$$

Figure 3 shows the mean-square tracking error given by Eq. (19) for various values of the measurement noise. The steady-state time-correlation function is

$$G(\tau) = \lim_{t \rightarrow \infty} E[e_{t+\tau} e_t] = \frac{\bar{D}}{B} \exp(-B\tau), \quad (20)$$

which may prove to be a useful result for performing fluorescence correlation spectroscopy (FCS) while tracking a sin-

²This not an unattainable experimental scenario if a particle is tracked, for example, by translating an excitation laser using acousto-optic modulators whose response bandwidth may exceed the particle's motional time scale by several orders of magnitude.

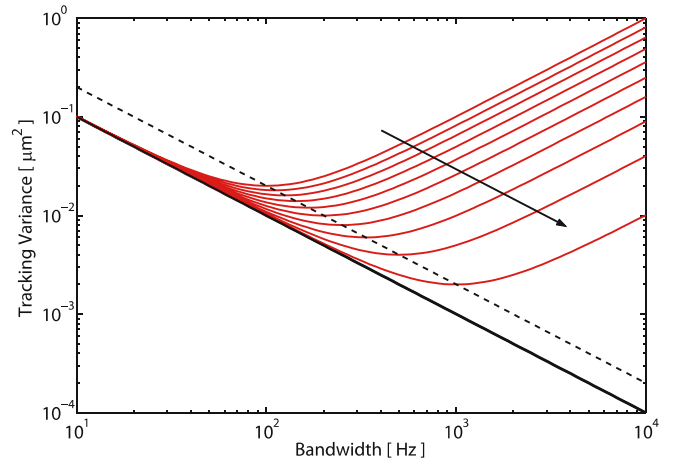


FIGURE 3 Mean-square tracking error $E[e_t^2]$ as a function of bandwidth B as predicted by Eq. (19) for $D = 1 \mu\text{m}^2/\text{s}$ and the noise spectral density ranging from $n_m = 10^{-2}$ to $n_m = 10^{-3} \mu\text{m}/\sqrt{\text{Hz}}$. The solid arrow indicates the direction of decreasing n_m . The solid black line is the zero-noise limit where the tracking error is D/B and the dashed line is the locus of minima in the tracking error given by Eqs. (21a) and (21b)

gle particle [10]. Equation (19) gives an asymptotic limit for particle localization with a simple first-order filtration of the demodulated fluorescence signal. The optimal bandwidth and estimator variance are given by

$$B_{\text{opt}} = \sqrt{2D}/n_m, \quad (21a)$$

$$E[e_t^2]_{\text{opt}} = \sqrt{2D}n_m. \quad (21b)$$

We could also have derived these bandwidth and localization results by applying a Kalman filter [14] to the system consisting of the particle's position X_t and a noisy measurement of that position (see the appendix). Since the Kalman filter is optimal in the mean-square sense, we see in this way that the simple first-order filtration at bandwidth B is in fact the optimal control law when the experimental response time is not a limiting factor.

Now suppose that we wish to track a particle's position and we require a squared tracking error (in the x direction) less than some value σ_x^2 . The maximum diffusion coefficient D_{max} for which a particle can be tracked within this tracking error constraint can be found by setting Eq. (21b) equal to σ_x^2 and using the full expression for the measurement noise n_m including a finite background:

$$D_{\text{max}} = \left(\frac{\Gamma_0 \sigma_x^4}{2w^2} \right) \left[\psi \left(\frac{r_0}{w} \right)^2 + 2 \frac{\Gamma_b}{\Gamma_0} \psi \left(\frac{\sqrt{2}r_0}{w} \right)^2 \right]^{-1}. \quad (22)$$

Equation (22) is an explicit expression for the largest diffusion coefficient D_{max} that can be tracked (in one dimension only) by fluorescence modulation; solving for σ_x , we find an expression for the smallest position variance that can be achieved when tracking a given diffusion coefficient. Note that at fixed r_0/w , D_{max} strictly decreases with increasing beam waist w ; however, at fixed fractional localization σ_x/w , D_{max} strictly increases with w .

Now consider tracking isotropic diffusion in three dimensions. This may be achieved by rotating the excitation laser

D	$\sigma (d=2)$	$\sigma (d=3)$
0.001	14	18
0.01	26	31
0.1	45	55
1.0	81	99
10.0	143	175
100.0	255	310

TABLE 1 Table showing the best possible standard deviation σ [nm] in localizing a particle with diffusion coefficient D [$\mu\text{m}^2/\text{s}$] ranging over relevant values for single-molecule spectroscopy in $d=2$ or 3 dimensions. The remaining parameters were fixed at $w = 0.5 \mu\text{m}$, $r_0 = w/\sqrt{2}$, $\Gamma_0 = 50 \text{ kHz}$, and $\Gamma_b = 10 \text{ kHz}$

in the xy plane and periodically modulating the focal depth in the z direction at a sufficiently different frequency that the three components may be demodulated separately (see for example Refs. [7, 8]). Let the measurement noise in the estimate of the x position be n_x and similarly for y and z . The total tracking error is given by the quadrature sum of the error in each dimension. Therefore, for three-dimensional localization such that the variance in distance from the origin is less than $\sigma^2 = \sigma_x^2 + \sigma_y^2 + \sigma_z^2$, the largest ‘trackable’ diffusion coefficient is

$$D_{\max} = \frac{\sigma^4}{2(n_x + n_y + n_z)^2}. \quad (23)$$

If the noise densities are equal in all directions, $n_x = n_y = n_z = n_m$, and we desire a variance in the distance to the origin less than σ^2 , then, in d dimensions, we have the general result

$$D_{\max} = \frac{\sigma^4}{2d^2 n_m^2} \iff \sigma_{\min} = (2Dd^2 n_m^2)^{1/4}. \quad (24)$$

A few values of the optimum localization $\sigma = \sigma_{\min}$ as a function of D are given in Table 1 for typical experimental parameters. The σ^4 scaling is quite steep, so that a moderate increase in the acceptable variance leads to a much larger ‘trackable’ diffusion coefficient; conversely, a moderate decrease in the acceptable variance strongly reduces the trackable diffusion coefficient.

Throughout this paper, we have assumed that a particle is tracked near the coordinate origin, so that linear approximations to $E[\hat{x}]$ and $\sigma_{\hat{x}}^2$ are accurate. However, before the final approximation, Eq. (13) is the exact variance for the linear estimator. We see that any deviations from the linear regime result in an estimator bias ($E[\hat{x}] \neq x$) and increased estimator noise (since $h_2(\varrho)$ is strictly positive away from the origin). Therefore, it is reasonable to assume that any tracking controller based on the linear position estimator \hat{x} will only perform worse than our linear approximation results when nonlinear correction terms are included in the noise density and estimator error. On the other hand, we cannot rule out the possibility that a more sophisticated, nonlinear signal processing scheme may be capable of exploiting the structure of $h_n(\varrho)$ in order to improve the tracking capability based on fluorescence modulation.

4 Numerical simulations

In the preceding sections, we developed a model for particle-tracking experiments in the presence of meas-

urement noise arising from photon-counting statistics. In our model, we linearized the demodulated fluorescence signal around the coordinate origin. This approximation is valid in the linear tracking regime in which the error in tracking a particle is well described by the model of Sects. 2 and 3. In this regime, the Ornstein–Uhlenbeck model of the tracking error is sufficient for describing the position of the particle, including the correlation statistics given by Eq. (20), which will be

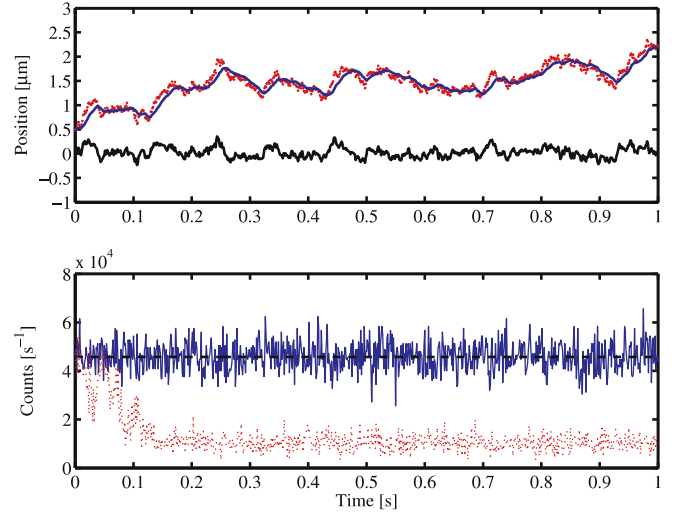


FIGURE 4 Two-dimensional tracking simulation in the linear regime. The position estimator \hat{X}_t and a particle with diffusion coefficient $D = 1 \mu\text{m}^2/\text{s}$ were started at the origin at time $t = 0$. The remaining parameters were $w = 532 \text{ nm}$, $r_0 = w/\sqrt{2}$, $\omega_0 = 2\pi \times 8000 \text{ Hz}$, $B = 100 \text{ Hz}$, $\Gamma_0 = 10^5 \text{ Hz}$, and $\Gamma_b = 10^4 \text{ Hz}$. The upper plot shows the x position of the particle X_t (red \cdot) and the position estimator \hat{X}_t (blue $-$), with the same offset added to each curve for clarity. Also shown is the tracking error e_t (black $-$). The lower plot shows the fluorescence count rate for this trajectory both with (blue $-$) and without (red \cdot) tracking control. The dashed curve is the expected fluorescence rate based on the linearized model, which is in good agreement with the full simulation

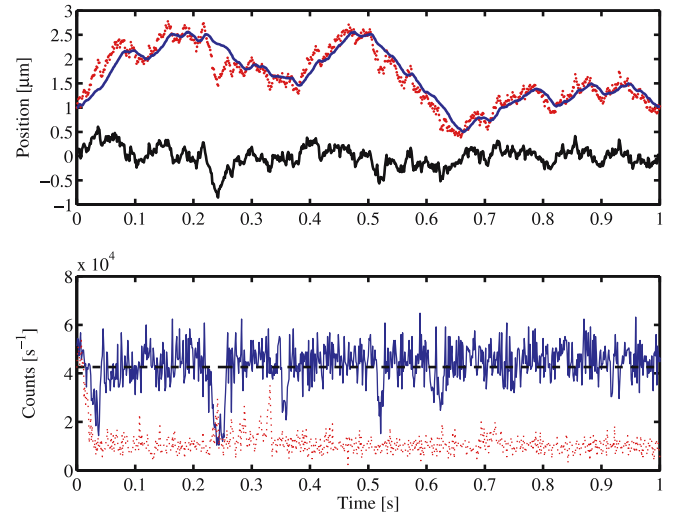


FIGURE 5 Two-dimensional tracking simulation in the nonlinear regime. The simulation parameters are the same as in Fig. 4, except that the particle’s diffusion coefficient was increased to $D = 2.5 \mu\text{m}^2/\text{s}$. In the nonlinear regime, the particle explores much more of the laser intensity, resulting in greater fluctuations of the tracking error e_t and the fluorescence intensity. The particle nearly escapes from the Gaussian laser but is recaptured a number of times during the simulation period

useful for performing FCS [10]. In a true experiment (with a Gaussian excitation laser), when the feedback bandwidth is either too low or too high, it may be impossible to localize a particle well enough to contain it within the linear regime. In some cases, it may not even be possible to contain the particle within the excitation laser focus so that it cannot be tracked at all; this is the untracked regime. Finally, there is an intermediate nonlinear tracking regime, in which a particle may be at least partially tracked, but it cannot be localized tightly enough to warrant the linearized model³. While the linear tracking and the untracked regimes may be treated exactly, using Ornstein–Uhlenbeck or free diffusion statistics, respectively, the nonlinear tracking regime is difficult to treat analytically. In this section, we present the results of numerical simulations across all of these regimes, both to illustrate the previously described statistics and to develop intuition about the intermediate nonlinear tracking regime.

The results of typical two-dimensional simulations are shown in Figs. 4 and 5. The simulations explicitly treat all aspects of the tracking process including particle diffusion, Poisson fluorescence statistics in a rotating Gaussian laser, lock-in detection at the rotation frequency, and translation of the laser centroid according to a bandwidth-limited filtration of the position estimate \hat{X}_t . Figure 4 shows an example of linear tracking, while Fig. 5 shows nonlinear tracking. See the figure captions for details of the simulation parameters. Qualitatively, we expect that the transition between the linear tracked regime and the untracked regime (passing through the nonlinear regime) occurs when the tracking error in the linear model reaches some threshold fraction of the beam waist w . Near this point in parameter space, a tracked (or partially tracked) particle may escape from the tracking laser and become untracked. Without calculating any details of escape probabilities, which would require a full nonlinear model of the tracking process, we can construct a qualitative picture of the transition between the linear and untracked regimes (treating the nonlinear tracking regime as a fuzzy boundary between the two). In Fig. 6 we explore the transition between the untracked and tracked regimes as a function of the feedback bandwidth B , with all other parameters held constant.

The simulation results displayed in Fig. 6 show that our qualitative picture of the transition between the linear and untracked regimes (detailed in the figure caption) agrees well with the actual behavior of the system. In this qualitative picture, the system exhibits threshold behavior, jumping discontinuously from the linear tracked regime to the untracked, free diffusion regime at points in parameter space where the squared tracking error calculated in the linear model exceeds some critical value, which we took to be $0.1w^2$. Using this rule, we may fix the experimental geometry and fluorescence parameters and construct a phase diagram in the space of the particle's diffusion coefficient D and the feedback bandwidth B indicating the boundaries between tracked and untracked regions. For tracking in d dimensions, we simply add the

³ We use the term ‘nonlinear’ in the regime where the position estimator \hat{X}_t , although a linear function of the measured fluorescence, is no longer a linear function of the particle's actual position X_t . In the language of control theory, we are using an optimal linearized control law outside its domain of applicability.

tracking errors from each Cartesian direction in quadrature. A tracking phase diagram constructed in this way is shown in Fig. 7.

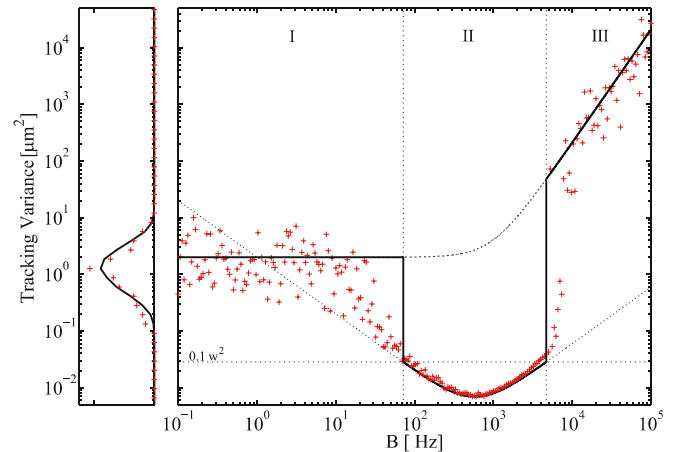


FIGURE 6 Two-dimensional ($d = 2$) Monte Carlo simulation results showing the mean (time-averaged) value of the squared tracking error ($\langle e_t^2 \rangle$) over a $T = 1$ s simulation. Regions I and III are untracked while region II is the linear tracked regime. The *solid black line* is a qualitative guide constructed as follows: in regions I and III, the *solid black curve* follows the free diffusion result ($\langle e_t^2 \rangle = d(D + n_B^2 B^2/2)T$) expected for free particle diffusion and estimator position driven by background fluorescence, while in region II the *solid black line* jumps to the expected value of the tracking error for the linear regime where the mean tracking error is $d\bar{D}/B$ independent of T . The jump point was conservatively chosen to be the bandwidth where the linear tracking error reaches $0.1w^2$; beyond this threshold value the simulations show that particles are at least partially tracked in the nonlinear regime, especially on the smaller B side. The expected distribution of free diffusion tracking errors (in the limit $B \ll \sqrt{D}/n_B$) is plotted on the *left*, together with a histogram of the simulated values with $B < 30$ Hz, showing that the points at the low-bandwidth end follow free diffusion statistics. In addition to reducing the average tracking error, linear tracking drastically reduces the variance in the tracking error. The remaining simulation parameters were $w = 532$ nm, $r_0 = w/\sqrt{2}$, $\omega_0 = 2\pi \times 10^5$ Hz, $D = 1 \mu\text{m}^2/\text{s}$, $\Gamma_0 = 5 \times 10^4$ Hz, and $\Gamma_b = 10^4$ Hz

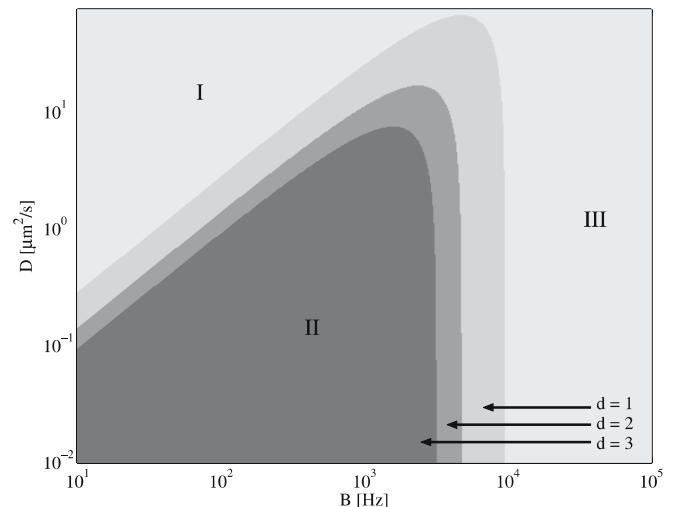


FIGURE 7 d -dimensional tracking phase diagram in the parameter space of diffusion coefficient D versus feedback bandwidth B , with all other parameters fixed. Regions I and III represent untracked phases where the feedback bandwidth is too slow and too fast, respectively. Region II is the linear tracking region. The nonlinear tracking region lies outside region II, extending into the untracked region. The simulations in Fig. 6 lie on a horizontal slice along the $D = 1 \mu\text{m}^2/\text{s}$ line of this phase diagram, with $d = 2$. All other parameters are the same as in Fig. 6

With this qualitative model, based on the exact statistics of the linear and untracked regimes and verified by numerical simulation in the nonlinear regime, we have succeeded in partitioning the experimental parameter space into ‘trackable’ and ‘untrackable’ regions.

5 Conclusions

In Sect. 2, we derived the noise spectral density n_m arising from photon-counting statistics in a fluorescence modulation particle-tracking scheme. We also showed the generic σ^4/n_m^2 dependence of the maximum trackable diffusion coefficient in a particle-tracking experiment subject to measurement noise, and combined these results to find explicit upper bounds on tracking performance for our own, and similar, experiments in Sect. 3. The steep scaling of D_{\max} with σ suggests that particle tracking by fluorescence modulation is useful for localizing a particle to a moderate fraction of the beam waist; however, it is very difficult to obtain high-resolution position information for particle tracking in the presence of measurement noise. Our calculations were performed for the case of two-dimensional tracking in a rotating Gaussian laser field; however, we attempted to partition the details of the experimental geometry into the function $\psi(x)$, while the remaining arguments are generically applicable to any linear position measurement of a diffusing particle subjected to measurement noise. Finally, in Sect. 4, we combined the analytical results of Sects. 2 and 3 with numerical simulations in the intermediate nonlinear tracking regime in order to verify a simple, qualitative procedure for determining the regions of parameter space in which a particle can be successfully tracked.

For future particle-tracking experiments, it will be crucial to understand the limits of particle tracking and particle localization by noisy fluorescence measurements. Although we have concentrated on the case of fluorescence modulation, any particle localization scheme based on fluorescence detection will be subject to some degree of measurement noise arising from the fundamental stochastic nature of photon-counting statistics. While the precise form of the noise will depend on all aspects of the experimental geometry and signal processing, most of the analysis in this paper will be applicable to these other cases.

ACKNOWLEDGEMENTS This work was supported by the Institute for Collaborative Biotechnologies through Grant No. DAAD19-03-D-0004 from the US Army Research Office and by the NSF through Grant Nos. DBI-0242705 and EIA-0323542.

Appendix: Optimal position estimation using a Kalman filter

In this appendix, we will show that Eqs. (21a) and (21b) arise naturally from a simple application of the Kalman filter. Consider the one-dimensional position X_t of a Brownian particle with diffusion coefficient D at time t , and consider an unfiltered measurement of this position, denoted by ξ_t , subject to a measurement noise density n_m . These quantities constitute a simple pair of coupled stochastic differential equations

$$dX_t = \sqrt{2D}dW_1, \quad (\text{A.1a})$$

$$\xi_t dt = X_t dt + n_m dW_2, \quad (\text{A.1b})$$

where dW_1 and dW_2 are uncorrelated Wiener increments, as in Eqs. (17). In the main text, we dealt only with the filtered estimate of the particle’s position given by \hat{X}_t . In the notation of this appendix, the unfiltered measurement ξ_t is proportional to the finite-windowed Fourier transform $\tilde{s}_t(\omega_0)$ of Sect. 2.

Assuming that the initial position of the particle is known, or is Gaussian distributed, we may apply a Kalman filter [14] to the system in Eqs. (A.1a) and (A.1b) to find the filtration of ξ_t , denoted by \hat{X}_t , that minimizes the mean-square error $e_t^2 = E[(\hat{X}_t - X_t)^2]$. The result of the Kalman filtration gives the following update rule for the estimate \hat{X}_t :

$$d\hat{X}_t = \frac{\sqrt{2D}}{n_m} (\hat{X}_t - \xi_t) dt. \quad (\text{A.2})$$

Eliminating $\xi_t dt$ in Eqs. (A.1a) and (A.2) results in the coupled system of equations (17) given in the body of the paper provided that we make the identification $B = \sqrt{2D}/n_m$. Thus, the optimal filtration of the position measurement ξ_t is in fact a first-order filtration with the filter bandwidth given by B_{opt} of Eq. (21a). The Kalman filter also describes the deterministic evolution of the estimator variance $E[(\hat{X}_t - X_t)^2]$ via an associated Riccati equation. Denoting this variance by Σ_t , the Riccati equation is

$$\frac{d\Sigma_t}{dt} = 2D - \frac{\Sigma_t^2}{n_m^2}, \quad (\text{A.3})$$

whose solution is

$$\Sigma_t = \sqrt{2D}n_m \tanh \left[\frac{\sqrt{2D}}{n_m} (t + t_0) \right], \quad (\text{A.4})$$

where t_0 parameterizes the initial uncertainty in the particle’s position. In the long-time limit, the stationary solution of Eq. (A.3) is easily seen to reproduce Eq. (21b).

REFERENCES

- 1 T. Ha, D.S. Chemla, T. Enderle, S. Weiss, *Appl. Phys. Lett.* **70**, 782 (1997)
- 2 J. Enderlein, *Appl. Phys. B* **71**, 773 (2000)
- 3 J. Enderlein, *Single Mol.* **1**, 225 (2000)
- 4 R.S. Decca, C.-W. Lee, S.R. Wassall, *Rev. Sci. Instrum.* **73**, 2675 (2002)
- 5 A.J. Berglund, H. Mabuchi, *Appl. Phys. B* **78**, 653 (2004)
- 6 S.B. Andersson, *Appl. Phys. B* **80**, 809 (2005)
- 7 V. Levi, Q. Ruan, K. Kis-Petikova, E. Gratton, *Biochem. Soc. Trans.* **31**, 997 (2003)
- 8 V. Levi, Q. Ruan, E. Gratton, *Biophys. J.* **88**, 2919 (2005)
- 9 M.A. Digman, C.M. Brown, P. Sengupta, P.W. Wiseman, A.R. Horowitz, E. Gratton, *Biophys. J.* **90**, 1317 (2005)
- 10 A.J. Berglund, H. Mabuchi, *Opt. Express* **13**, 8069 (2005)
- 11 A. Yildiz, J.N. Forkey, S.A. McKinney, T. Ha, Y.E. Goodman, P.R. Selvin, *Science* **300**, 2061 (2003)
- 12 N.G. van Kampen, *Stochastic Processes in Physics and Chemistry* (Elsevier Science/North-Holland, Amsterdam 2001)
- 13 C.W. Gardiner, *Handbook of Stochastic Methods for Physics, Chemistry and the Natural Sciences*, 2nd edn. (Springer, Berlin 1985)
- 14 O.L.R. Jacobs, *Introduction to Control Theory*, 2nd edn. (Oxford University Press, Oxford 1996)